

An adaptive element subdivision method for evaluation of weakly singular integrals in 3D BEM

Jianming Zhang*, Chenjun Lu, Xiuxiu Zhang, Guizhong Xie, Yunqiao Dong, Yuan Li
(State Key Laboratory of Advanced Design and Manufacturing for Vehicle Body, Hunan University, Changsha 410082, China)

*Correspondence to: Jianming Zhang

College of Mechanical and Vehicle Engineering, Hunan University, Changsha 410082, China

Telephone: +86-731-88823061

E-mail: zhangjm@hnu.edu.cn

Abstract: A general adaptive element subdivision method is presented for the numerical evaluation of weakly singular integrals in three-dimensional boundary element analyses. In our method, the element is subdivided into a number of patches through a sequence of spheres with decreasing radius. The patches obtained by our method are automatically refined as they approaching the source point. Consequently, each patch is “good” in shape and size for standard Gaussian quadrature, and hence high accuracy can be achieved by a small number of Gaussian sample points. Our method is applicable to any shape of element with arbitrary location of the source point inside, at vertices or on edges of the element. Numerical examples are presented for planar and curved surface elements. The results demonstrate that our method can provide much better accuracy and efficiency than the conventional subdivision method.

Keywords: *BEM, weakly singular integral, element subdivision, Gaussian quadrature.*

1. Introduction

It is well-known that accurate calculation of weakly singular integrals is of crucial importance for successful implementation of the boundary element method (BEM) [1-8]. Element subdivision is one of the most widely used methods for nearly or weakly singular integration. In the conventional subdivision method, the sub-elements which are also called patches are obtained by simply connecting the singular point with each vertex of the element [9]. Kane has proposed the reusable intrinsic sample point algorithm which employed a discrete number of sets of predetermined, customized, near-optimum, sample point quantities associated with the intrinsic boundary element [10]. This algorithm was performed using a predefined element subdivision template. Some other subdivision schemes have also been applied for discontinuous elements [11] by Banerjee. Zhang et al have used the conventional subdivision method coupled with a new coordinate transformation to remove singularities [12] and further developed an adaptive element subdivision method named Quad-tree subdivision [13] (see Fig. 1). All the above mentioned methods are performed in the local coordinate system of the element rather than in the physical coordinate system. Obviously, it may produce patches in “bad” shapes in case the element are

curved or distorted or the element is irregular in shape. As patches in good shape in the parametric space may become bad when they are mapped into the physical coordinate system. Even for planar and regular elements, if discontinuous element is adopted, the patches obtained by the conventional method cannot be guaranteed to be suitable for Gaussian integration rules. For example, Fig. 2 shows a boundary mesh of a body with a fillet face. The elements shown in Fig. 3 are taken from the mesh shown in Fig. 2. The subdivision (a) in Fig. 3 is for a continuous element, and (b) and (c) are for discontinuous elements. Numerical tests have demonstrated that, with the same number of Gaussian sample points ($6 \times 6 = 36$), the accuracy of integration with the $1/r$ kernel on patches (a)-②, (b)-④ and (c)-④ is less than $1.0E-5\%$, on patch (a)-① is 0.05% , which is acceptable, but on patches (b)-①, (b)-②, (b)-③, (c)-① and (c)-② is bigger than 1% , which is completely wrong. From this example, it is seen that much attention should be paid to the subdivision scheme, particularly in case discontinuous elements are adopted in the BEM implementation.

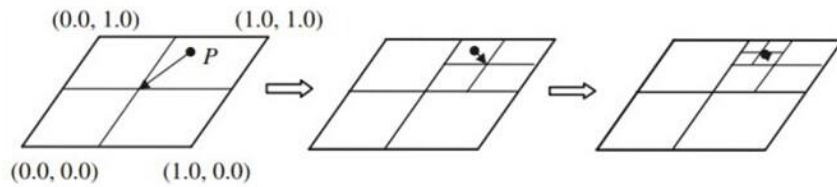


Figure 1. The Quadtree subdivision of an element.

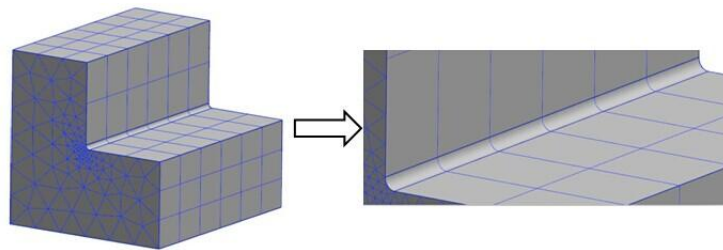


Figure 2. Slender Curved elements on the fillet face.

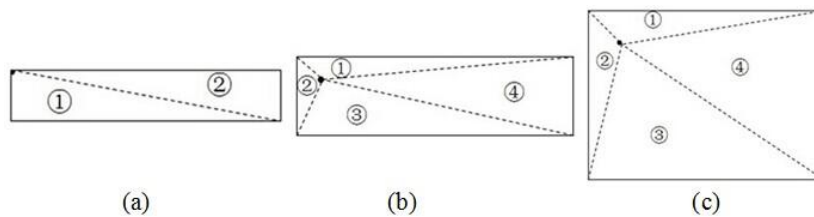


Figure 3. Patches obtained by the conventional subdivision method.

In this paper, a general adaptive element subdivision method called Sphere Subdivision Method is proposed. In proposed method, elements are not subdivided in the element local coordinate system but in the physical coordinate system. An element is subdivided into a number of patches through a sequence of spheres with decreasing radius, and the obtained patches are automatically refined as they approaching the source point. Therefore, each patch is ensured to be “good” in shape and size for standard Gaussian quadrature (The word “good” here means that the

area of the patch is as large as possible under the condition that the fundamental solution within the patch can be accurately interpolated by low order polynomials). Our method is applicable to any shape of elements, no matter where the source point is located, namely, it's suitable for both continuous and discontinuous elements. Detailed description of sphere subdivision method is presented in Section 2. In Section 3, numerical examples for planar and curved surface elements are presented to demonstrate that high accuracy can be achieved by a small number of Gaussian points with the proposed method.

2. Adaptive element subdivision method

To achieve the best balance between accuracy and efficiency, it is desirable that subdivided patches closer to the source point have relatively smaller sizes. To guarantee this, we use a sequence of sphere centered at the source point with decreasing radius to cut the element, recursively. With this method, no matter where the position of the source point is located in the element, patches with “good” shape can always be obtained. Since this subdivision method is performed in the physical coordinate system, it is a common algorithm for every kind of element. Before describing our method, we define some symbols first.

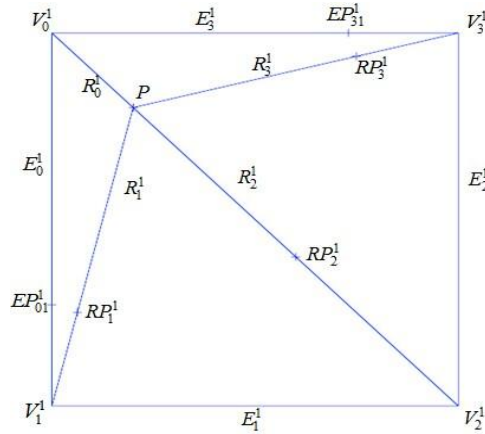


Figure 4. First step of element subdivision.

For a 3D boundary element in which the source point is located, as shown in Fig. 4, the following symbols are defined:

P ——the source point;

V_i^j ——the i -th vertex in the j -th step;

E_i^j ——the i -th edge in the j -th step;

R_i^j ——the line segment connecting P and V_i^j ;

EP_{ik}^j ——the k -th intersection of E_i^j with the j -th sphere, $k=1, 2$;

RP_i^j ——intersection of R_i^j with the j -th sphere;

L_i^j ——distance between p and V_i^j ;

D_i^j — distance between p and E_i^j ;

Let $L_{max} = \max \{L_i^j, D_i^j\}$, $L_{min} = \min \{L_i^j, D_i^j\}$ ($L_{min} \neq 0$).

In each step, a sphere is constructed with its center at P , and its radius is defined as:

$$r_j = \eta^j * L_{max} \quad (1)$$

where η is empirical value. In this study, η is taken as 0.25.

Taking the first step for example, as shown in Fig. 5, a sphere is constructed centered on P and then intersections of sphere and lines, i.e. points $EP_{01}^1, RP_1^1, RP_2^1, RP_3^1$ and EP_{31}^1 , are connected in order. Patches are obtained as shown in Fig. 6. At the same time, intersections take the place of the original vertexes to be new vertexes in the next step, and edges have also been renewed for the next step. Repeat this process and a certain number of new patches will be obtained after each step. This algorithm is similar to advancing front method which needs to update vertexes and edges in every step [14].

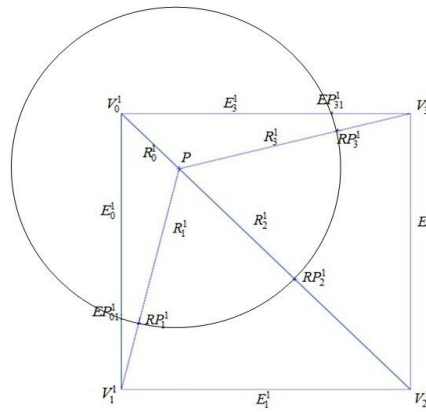


Figure 5. A sphere is constructed centered on P .

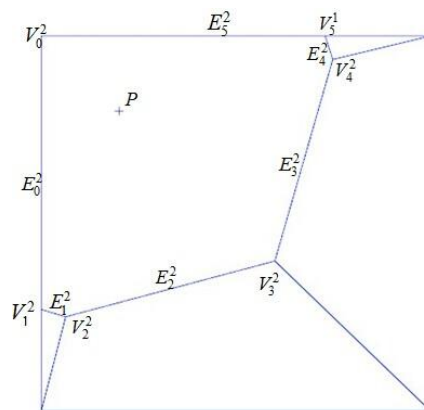


Figure 6. Patches obtained after the first step.

As the procedure repeating, the value of r_j gradually decreases. It is possible that the following situation as shown in Fig. 7 occurs, in which two points of intersection are too close to

obtain patches with “good” shape or size.

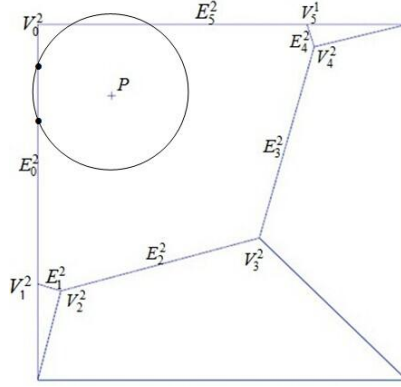


Figure 7. The situation we are trying to avoid that the two intersections are too close.

To avoid this situation, a solution is put forward: when $r_j < \eta_{Min} * L_{min}$, where $\eta_{Min} = \sqrt{2}$, the intersections and the source point will be connected as illustrated in Fig. 9(c) and the procedure stops cycling. By now, all the patches are obtained. For the patches containing source point, an α - β transformation is used to eliminate the singularities [12]. The α - β transformation is expressed as follows:

$$\begin{cases} x_a = x_0 + (x_1 - x_0)\alpha \\ y_a = y_0 + (y_1 - y_0)\alpha \end{cases} \quad (2a)$$

$$\begin{cases} x_b = x_0 + (x_2 - x_0)\alpha \\ y_b = y_0 + (y_2 - y_0)\alpha \end{cases} \quad (2b)$$

$$\begin{cases} x = x_a + (x_b - x_a)\beta \\ y = y_a + (y_b - y_a)\beta \end{cases} \quad \alpha, \beta \in [0,1] \quad (2c)$$

Combining Eqs. (2a), 2(b) and (2c), the expression for obtaining the Cartesian coordinates x and y can be written as:

$$\begin{cases} x = x_0 + (x_1 - x_0)\alpha + (x_2 - x_1)\alpha\beta \\ y = y_0 + (y_1 - y_0)\alpha + (y_2 - y_1)\alpha\beta \end{cases} \quad (3)$$

The Jacobian of the transformation from the x - y system to the α - β system is αS , where

$$S = |x_0y_1 + x_1y_2 + x_2y_0 - x_0y_2 - x_1y_0 - x_2y_1| \quad (4)$$

and S keeps constant over the triangle.

From Eq. (2) to Eq. (4), it can be noted that the new coordinate system is much simpler to implement than the polar coordinate system. This is due to the fact that both α and β are constrained to the interval $[0, 1]$ in each triangle, thus there is no need to calculate their spans.

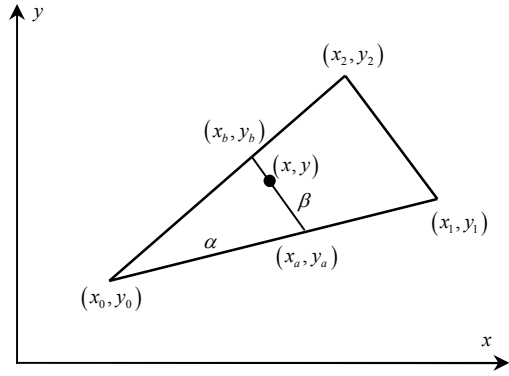


Figure 8. The α - β coordinate transformation.

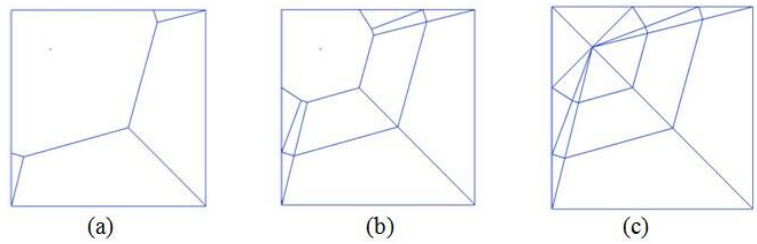


Figure 9. Patches obtained in subdivision steps: (a) the first step; (b) the second step; (c) the last step.

The main algorithm for creating patches is described by the following flow chart shown in Fig. 10.

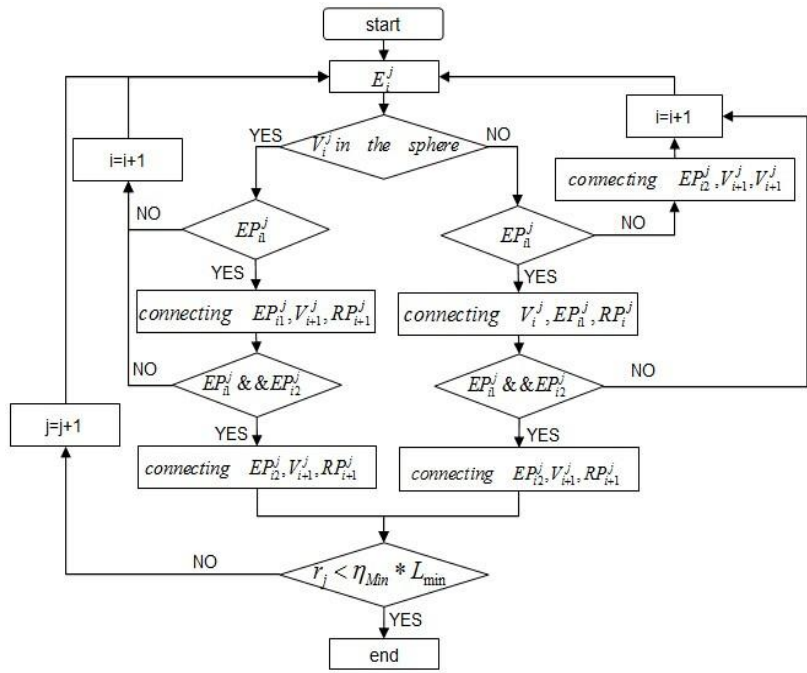


Figure 10. Flow chart of subdivision algorithm.

There are two factors that considerably decrease the accuracy of α - β transformation for

patches containing source point. First, the lengths of two adjacent edges intersecting at the source point differ largely, but from the description of the procedure above, it can be easily seen that this case will not happen in our method. Second, angle between two adjacent edges which intersect at the source point is larger than expected. In this case, each patch containing a large angle will be divided into two patches, until all angles meet the condition $\text{angle} < \text{diviAngle}$, where diviAngle is defined in the procedure.

The other two problems can be seen from Fig. 9(c). Firstly, although the lengths of two adjacent edges of the patch are almost equal and the angles are small enough, total number of patches is very large which will cause much greater computational cost. Secondly, shapes of some patches without containing the source point are “bad”. In order to deal with these problems, merging operation will be introduced next.

The merging operation will be used in three cases. Firstly, in a certain step, if the distance between EP_{ik}^j and the vertex is smaller than an expected value d_1 , EP_{ik}^j will be moved to the adjacent vertex. Secondly, If the distance between RP_i^j and the vertex is smaller than an expected value d_2 , RP_i^j will be moved to the adjacent vertex. Thirdly, if the distance between RP_i^j and EP_{ik}^j is smaller than an expected value d_3 , RP_i^j will be moved to EP_{ik}^j .

d_1 、 d_2 、 d_3 are defined as follows:

$$d_1 = \text{edgeFactor} * d(V_i^j, V_{i+1}^j)$$

$$d_2 = \text{radFactor} * r_j$$

$$d_3 = \text{radFactor} * r_j$$

where $\text{edgeFactor}=0.1$ and $\text{radFactor}=0.1$. After the merging operation, new patches are obtained, as Fig. 11 depicts. We can see the number of patches is reduced and the shapes of patches are improved obviously compared with that in Fig. 9.

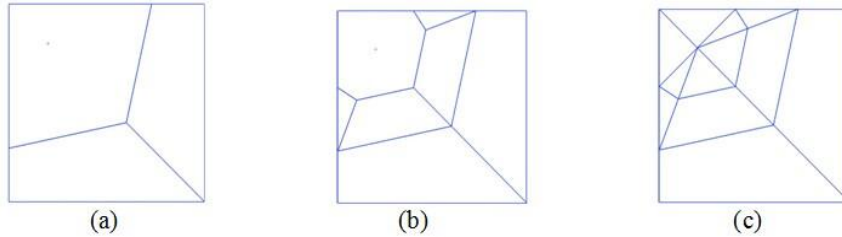


Figure 11. Element subdivision after merging operation: (a) the first step; (b) the second step; (c) the last step.

With the detailed description above, it can be clearly seen that our method has obvious advantages over conventional method. Firstly, the patches containing source point have much better shape than those obtained by conventional subdivision method [1], while the remaining patches also have better shape due to the properties of sphere and merging operation. Secondly, as the patches obtained are automatically refined as they approaching the source point, Gaussian

sample points are set denser around the source point to get an accurate enough result. Away from the source point, Gaussian sample points are sparsely distributed, much fewer but enough to grantee an accurate result, so a large number of unnecessary Gaussian sample points are avoided. In the whole process, the number of patches and their size are determined adaptively by the position of singular point. In a word, with the adaptive element subdivision method coupled with the α - β transformation, the weakly singular integrals can be solved with higher accuracy and less computational cost. It should be noted that all the intersection points should be projected from physical coordinate system to element local coordinate system in this algorithm.

3. Numerical examples

To evaluate the effectiveness and accuracy of our method, in this section, several comparisons are made between our method and the conventional method for planar element and curved surface element. For the purpose of error estimation, relative error is defined as follows:

$$\text{Relative Error} = \left| \frac{I_n - I_e}{I_e} \right| \quad (5)$$

where I_n is the numerical solution, and I_e is the exact solution of the integral.

We consider the numerical evaluation of the integral

$$I = \int_{\Gamma} \frac{1}{4\pi r} d\Gamma \quad (6)$$

In all the numerical examples, the α - β transformation is used to remove singularities in the patches which contain the source point, while the remaining regular quadrilateral and triangular patches are respectively evaluated by the standard Gaussian quadrature and Hammer quadrature. **The number of the Gaussian points m is determined by [15-17]**

$$m = \sqrt{\frac{2}{3}p + \frac{2}{5}} \left[-\ln(e/2)/10 \right] \left[\left(\frac{8L}{3r_j} \right)^{\frac{3}{4}} + 1 \right] \quad (7)$$

where p represents the order of the singularity ($p=1,2,3$). e denotes the error tolerance. L is the length of patch in integral direction. And r_j is the sphere radius defined in Eq. (1).

3.1 Examples of planar element

In this part, adaptive element subdivision and corresponding numerical result are presented for planar quadrilateral element and slender element. Vertex coordinates of planar quadrilateral element are (1, 1), (-1, 1), (-1, -1), (1, -1) in the physical coordinate system, while vertex coordinates of slender element are (10, 1), (0, 1), (0, 0), (10, 0). As Fig. 12(a) and Fig. 13(a) show, the source points are almost coincident with the vertexes, with their coordinates are (0.99, 0.9) and (9.0, 0.9) respectively. As Fig. 12(b) and Fig. 13(b) show, the source points are very close to the edges, with their coordinates are (0.0, 0.99) and (5.0, 0.9) respectively.

Fig. 12 and Fig. 13 show patches obtained with our method. On the right of each figure is the partial enlarged view of the part containing source point, from which we can see the patches of

both planar quadrilateral element and slender element are in “good” shapes and size.

The accuracy obtained by both our method and the conventional method and the number of the Gaussian sample points used are listed in Table 1 and Table 2 for different locations of the source point. It is seen that to obtain the same level of accuracy, our method needs much fewer sample points, and thus, considerably increases the computational efficiency. On the other hand, when the number of Gaussian sample points used is the same, the accuracy obtained by our method is 5 to 7 orders of magnitude higher than that by the conventional method.

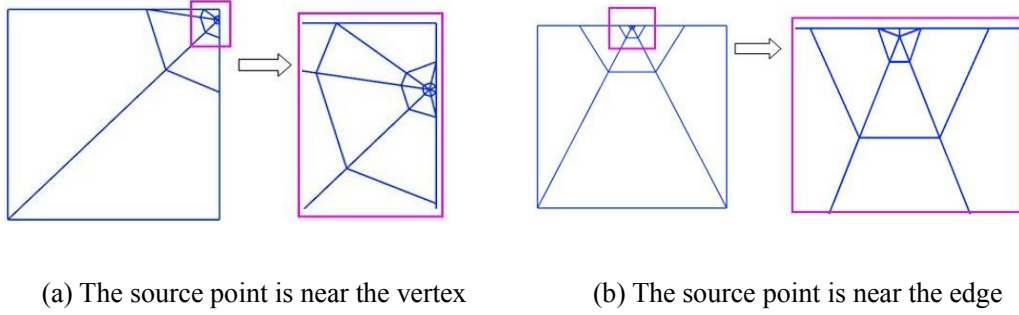


Figure 12. Subdivisions of planar quadrilateral element with our method.

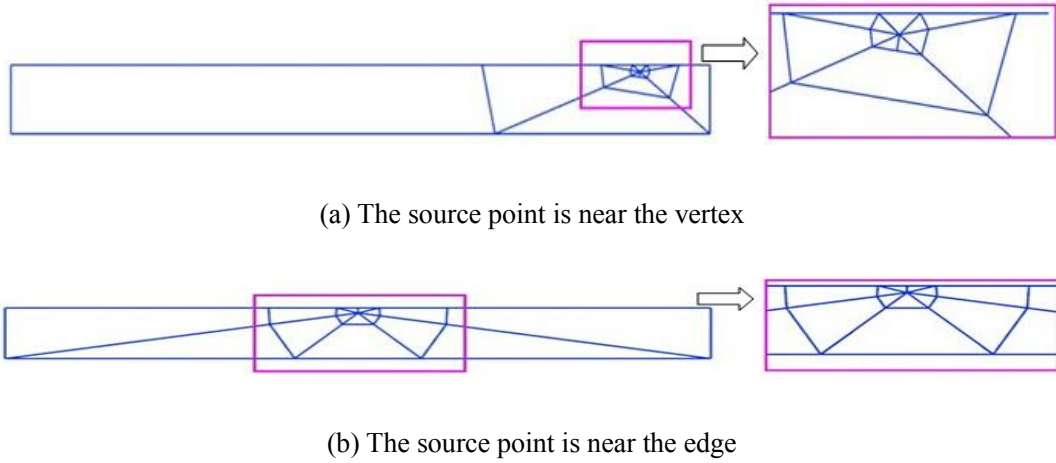


Figure 13. Subdivisions of planar slender element with our method.

Table 1: Numerical evaluation for planar element using the same number of Gaussian sample points.

Planar element	Source point	Gaussian points number		Relative Error	
		Conventional method	Our method	Conventional method	Our method
quadrilateral	(0.99,0.9)	1200	1195	4.46e-004	2.37e-009
	(0.0,0.99)	1200	1191	2.10e-003	1.21e-010
slender	(9.0,0.9)	1200	1197	3.73e-004	1.35e-009
	(5.0, 0.9)	1200	1194	3.55e-003	3.66e-008

Table 2: Numerical evaluation for planar element with Relative Error of the same order of magnitude

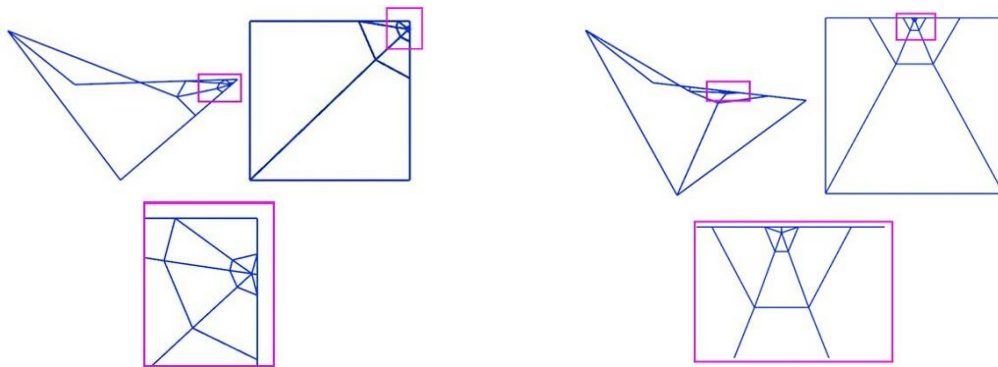
Planar element	Source point	Gaussian points number		Relative Error	
		Conventional method	Our method	Conventional method	Our method
quadrilateral	(0.99,0.9)	6000	1209	3.30e-009	3.25e-009
	(0.0,0.99)	12000	843	1.77e-008	3.35e-008
slender	(9.0,0.9)	5200	1173	2.57e-010	2.74e-010
	(5.0, 0.9)	6000	834	1.19e-007	1.89e-007

3.2 examples of curved surface element

In this part, adaptive element subdivision and corresponding numerical result are presented for curved surface quadrilateral element and curved slender element. Vertex coordinates of the curved surface quadrilateral element are $(1, 1, 1)$, $(-1, 1, 0)$, $(-1, -1, 1)$, $(1, -1, 0)$, while vertex coordinates of the curved slender element are $(10, 1, 0.5)$, $(0, 1, 0)$, $(0, 0, 0.5)$, $(10, 0, 0)$. As Fig. 14(a) and Fig. 15(a) show, the source points are almost coincident with the vertexes, with their coordinates are $(0.99, 0.9, 0.9455)$ and $(9.5, 0.95, 0.4525)$ respectively. As Fig. 14(b) and Fig. 15(b) show, the source points are very close to the edges, with their coordinates are $(0.0, 0.99, 0.5)$ and $(5.0, 0.9, 0.25)$ respectively.

Fig. 14 and Fig. 15 show patches obtained with our method. On the upper right of each figure is a top view of the curved element. At the bottom is the enlarged view of the part containing source point. From the Fig. 14 and Fig. 15, we can see the patches of both curved quadrilateral element and slender element are in “good” shapes and size.

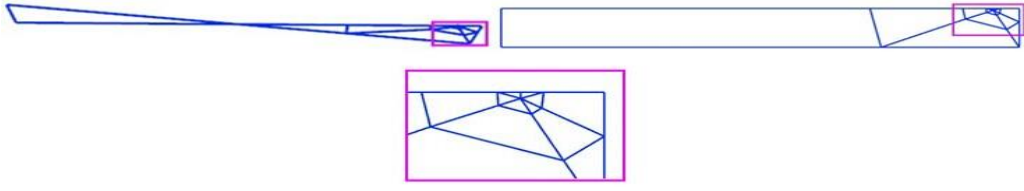
The accuracy obtained by both our method and the conventional method and the number of the Gaussian sample points used are listed in Table 3 and Table 4 for different locations of the source point. From Table 3, it is seen that when the number of Gaussian sample points used is the same, the accuracy obtained by our method is 5 to 7 orders of magnitude higher than that by the conventional method. From Table 4, it is seen that to obtain the same level of accuracy, our method needs much fewer sample points, and thus, considerably increases the computational efficiency. The effectiveness and accuracy of our method are demonstrated again.



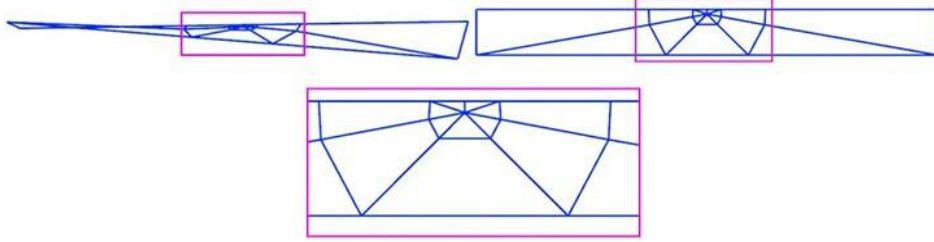
(a) The source point is near the vertex

(b) The source point is near the edge

Figure 14. Subdivisions of curved quadrilateral element with our method.



(a) The source point is near the vertex



(b) The source point is near the edge

Figure 15. Subdivisions of curved slender element with our method.

Table 3: Numerical evaluation for curved element using the same number of Gaussian sample points.

Curved surface element	Source point	Gaussian points number		Relative Error	
		Conventional method	Our method	Conventional method	Our method
quadrilateral	(0.99,0.9,0.9455)	1200	1189	5.74e-004	1.14e-009
	(0.0, 0.99,0.5)	1200	1197	2.33e-003	1.48e-009
slender	(9.5,0.95,0.4525)	1200	1200	1.28e-003	1.97e-010
	(5.0, 0.9,0.25)	1200	1194	3.50e-003	3.58e-008

Table 4: Numerical evaluation for curved element with Relative Error of the same order of magnitude

Curved surface element	Source point	Gaussian points number		Relative Error	
		Conventional method	Our method	Conventional method	Our method
quadrilateral	(0.99,0.9,0.9455)	6000	1225	5.84e-008	1.01e-008
	(0.0, 0.99,0.5)	16000	1039	1.48e-008	5.11e-008
slender	(9.5,0.95,0.4525)	6000	997	6.43e-009	5.09e-009
	(5.0, 0.9,0.25)	5400	822	4.13e-007	2.46e-007

The results demonstrate that shapes of the patches for both planar and curved surface element are “good” with the proposed adaptive element subdivision method. Moreover, our method can provide higher accuracy and efficiency than the conventional method with fewer Gaussian sample points.

4. Conclusions and future work

A general adaptive element subdivision method for the numerical evaluation of weakly singular integrals on 3D boundary element was proposed in this paper. With a sequence of spheres and the merging operation, patches with “good” shape can be obtained for both planar and curved surface boundary element with the proposed method, no matter where the singular point is located. From the numerical examples, it has been demonstrated that comparing with the conventional method, the accuracy of results has been significantly improved by using the proposed method. On the other hand, to obtain the same level of accuracy, our method requires much fewer sample points, and thus, considerably increases the computational efficiency. Extension of our work to 3D nearly singular integral is ongoing.

Acknowledgement

This work was supported in part by National Science Foundation of China under grant number 11172098, in part by Hunan Provincial Natural Science Foundation for Creative Research Groups of China under grant number 12JJ7001, in part by Open Research Fund of Key Laboratory of High Performance Complex Manufacturing, Central South University under grant number Kfkt2013-05.

References

- [1] Zhang JM, Tanaka M, Matsumoto T. Meshless analysis of potential problems in three dimensions with the hybrid boundary node method. *Int J Numer Meth Eng* 2004; 59(9): 1147-1166.
- [2] Liu YJ. Analysis of shell-like structures by the boundary element method based on 3-D elasticity: formulation and verification. *Int J Numer Meth Eng* 1998; 41(3): 541-558.
- [3] Xie GZ, Zhou FL, Zhang JM, Zheng XS, Huang C. New variable transformations for evaluating nearly singular integrals in 3D boundary element method. *Eng Anal Bound Elem* 2013; 37(9): 1169-1178.
- [4] Ma H, Kamiya N. Distance transformation for the numerical evaluation of near singular boundary integrals with various kernels in boundary element method. *Eng Anal Bound Elem* 2002; 26(4): 329-339.
- [5] Gao XW, Yang K, Wang J. An adaptive element subdivision technique for evaluation of various 2D singular boundary integrals. *Eng Anal Bound Elem* 2008; 32(8): 692-696.
- [6] Niu ZR, Wendland WL, Wang XX, Zhou HL. A sim-analytic algorithm for the evaluation of the nearly singular integrals in three-dimensional boundary element methods. *Comput Methods Appl Mech Eng* 2005; 31:949-64.
- [7] Cheng AHD, Detournay E. On singular integral equations and fundamental solutions of poroelasticity. *Int J Solids Struct* 1998; 35(34): 4521-4555.
- [8] Zhang YM, Gu Y, Chen JT. Boundary layer effect in BEM with high order geometry elements using transformation. *CMES-Comput. Model. Eng. Sci* 2009b; 45(3): 227.
- [9] Klees R. Numerical calculation of weakly singular surface integrals. *J Geodesy* 1996; 70(11): 781-797.
- [10] Kane JH, Gupta A, Saigal S. Reusable intrinsic sample point (RISP) algorithm for the efficient numerical integration of three dimensional curved boundary elements. *Int J Numer Meth Eng* 1989; 28(7): 1661-1676.
- [11] Banerjee PK, Butterfield R. *Boundary element methods in engineering science*. London: McGraw-Hill, 1981.
- [12] Zhang JM, Qin XY, Han X, Li GY. A boundary face method for potential problems in three dimensions. *Int J Numer Meth Eng* 2009; 80(3): 320-337.

- [13]Tanaka M, Zhang JM, Matsumoto T. Boundary-type meshless solution of potential problems: comparison between singular and regular formulations in hybrid BNM Transactions of JASCOME, Journal of Boundary Element Methods 2003; Vol.20, pp.21-26.
- [14]Wu B, Wang S. Automatic triangulation over three-dimensional parametric surfaces based on advancing front method. Finite Elem Anal Des 2005; 41(9): 892-910.
- [15]Gao XW, Davies T G. Adaptive integration in elasto-plastic boundary element analysis. Journal of the Chinese institute of engineers 2000; 23(3): 349-356.
- [16]Bu S, Davies TG. Effective evaluation of non-singular integrals in 3D BEM. Advances in Engineering Software 1995; 23(2): 121-128.
- [17]Lachat JC, Watson JO. Effective numerical treatment of boundary integral equations: A formulation for three-dimensional elastostatics. International Journal for Numerical Methods in Engineering 1976;10(5): 991-1005.